Rate of Access to the Binding Sites in Organically Modified Silicates. 2. Ordered Mesoporous Silicas Grafted With Amine or Thiol Groups

ARTICLE *in* CHEMISTRY OF MATERIALS · MAY 2003

Impact Factor: 8.35 · DOI: 10.1021/cm021310e

3 AUTHORS, INCLUDING:

Mathieu Etienne
French National Centre for Scientific Research
92 PUBLICATIONS **2,184** CITATIONS
SEE PROFILE

Bénédicte Lebeau
Université de Haute-Alsace
172 PUBLICATIONS **5,200** CITATIONS
SEE PROFILE

Rate of Access to the Binding Sites in Organically Modified Silicates. 2. Ordered Mesoporous Silicas Grafted with Amine or Thiol Groups

Alain Walcarius,*,† Mathieu Etienne,† and Bénédicte Lebeau‡

Laboratoire de Chimie Physique et Microbiologie pour l'Environnement, Unité Mixte de Recherche UMR 7564, CNRS−Université H. Poincaré Nancy I, 405, rue de Vandoeuvre, F-54600 Villers-les-Nancy, France, and Laboratoire de Matériaux Minéraux, UMR 7016, CNRS−Ecole Nationale Supérieure de Chimie de Mulhouse, 3, rue Alfred Werner, F-68093 Mulhouse Cedex, France

Received September 23, 2002. Revised Manuscript Received February 17, 2003

Five different ordered mesoporous silica samples displaying various pore sizes and structures (two small-pore MCM-41, two large-pore MCM-41, and one small-pore MCM-48) and one amorphous silica gel have been grafted with either aminopropyl or mercaptopropyl groups. The resulting aminopropyl-grafted silicas (APS) and mercaptopropyl-grafted silicas (MPS) have been studied in solution via protonation of APS and metal ion binding on both APS and MPS. Special attention was given to characterize the accessibility to the binding sites and to the speed at which the reactants are reaching these reactive centers inside the mesoporous materials. Results have been obtained from batch experiments, by monitoring the reactant depletion in suspensions containing APS or MPS particles, and discussed with respect to the structure and porosity of the organic−inorganic hybrids. As a general trend, both accessibility and rate of access to the reactive sites were higher with ordered mesoporous solids than with amorphous materials of comparable porosity (average pore size ∼60−70 Å). The ordered mesoporous structures of smaller pore size (∼35 Å) gave rise to the same performance as that of large-pore amorphous silica, only if pore blocking can be avoided during the grafting process; if not, the advantage of uniform pore structure over the corresponding amorphous material did not exist anymore: a pore volume of at least 0.5 cm^3 g^{-1} remaining upon grafting was necessary to keep this advantage. Increasing the amount of grafted moieties in the mesopores also led to restricted mass-transfer rates because of increasing steric hindrance. Moreover, protonation of mesoporous APS displaying uniform-sized channels was found to be dramatically slow at protonation levels higher than 50%, leading even to less-than-complete occupancy levels after 24 h of equilibration, most probably because of strong repulsive electrostatic interactions in such a confined medium. Applying a simplified diffusion model, the access rates of Cu^{II} in APS and Hg^{II} in MPS materials were quantified via calculation of apparent diffusion coefficients, D_{app}, by appropriate fitting of kinetic curves. D_{app} values were found to decrease slowly upon gradual completion of reaction because progressively less space was available for the ingress of reactants upon filling the mesostructures. This work would help at selecting the most appropriate conditions for target applications of grafted mesoporous solids in terms of capacity, accessibility, and especially, access rates to the active sites.

1. Introduction

The discovery of the first mesoporous silica featuring a (hexagonal) pore-ordered system, which was obtained using a surfactant as the structure-directing agent,[1] constitutes a milestone in the field of porous materials.[2−7] This pioneering work[1] has generated huge efforts of research in both synthesis and inclusion chemistry of new mesoporous materials with various composition and structure,[2] offering new opportunities for applications

* Corresponding author. Fax: (+33) 3 83 27 54 44. E-mail: walcariu@lcpe.cnrs-nancy.fr.

† CNRS−Université H. Poincaré Nancy I.

‡ CNRS−Ecole Nationale Supérieure de Chimie de Mulhouse.

(1) (a) Kresge, C. T.; Leonowicz, M. E.; Roth, W. J.; Vartuli, J. C.; Beck, J. S. *Nature* **1992**, *359*, 710. (b) Beck, J. S.; Vartuli, J. C.; Roth, W. J.; Leonowicz, M. E.; Kresge, C. T.; Schmitt, K. D.; Chu, C. T.-W.; Olson, D. H.; Sheppard, E. W.; McCullen, S. B.; Higgins, J. B.; Schlenker, J. L. *J. Am. Chem. Soc.* **1992**, *114*, 10834.

(2) (a) Beck, J. S.; Vartuli, J. C. *Curr. Opin. Solid State Mater. Sci.* **1996**, *1*, 76. (b) Brinker, C. J. *Curr. Opin. Solid State Mater. Sci.* **1996**, *1*, 798. (c) Zhao, X. S.; Lu, G. Q.; Millar, G. J. *Ind. Eng. Chem. Res.* **1996**, *35*, 2075. (d) Raman, N. K.; Andersen, M. T.; Brinker, C. J. *Chem. Mater.* **1996**, *8*, 1682. (e) Goltner, C. G.; Antonietti, M. *Adv. Mater.* **1997**, *9*, 431. (f) Zhao, D.; Feng, J.; Huo, Q.; Melosh, N.; Fredrickson G. H.; Chmelka, B. F.; Stucky, G. D. *Science* **1998**, *279*, 548. (g) Ciesla, U.; Schüth, F. *Microporous Mesoporous Mater.* **1999**, *27*, 131. (h) Stein, A.; Melde, B. J. *Surf. Sci. Ser.* **2001**, *100*, 819. (i) Oye, G.; Sjoblom, J.; Stocker, M. *Adv. Colloid Interface Sci.* **2001**, *89*−*90*, 439. (j) He, X.; Antonelli, D. *Angew. Chem., Int. Ed.* **2002**, *41*, 214. (k) Soten, I.; Ozin, G. A. In *Supramolecular Organization and Materials Design*; Jones, W., Rao, C. N. R., Eds.; Cambridge University Press: Cambridge, 2002; pp 34−82.

(3) (a) Corma, A. *Chem. Rev.* **1997**, *97*, 2373. (b) Corma, A.; Kumar, D. *Stud. Surf. Sci. Catal.* **1998**, *117*, 201. (c) Corma, A. *Top. Catal.* **1998**, *4*, 249.

10.1021/cm021310e CCC: $25.00
Published on Web 05/06/2003

in various fields, including mainly heterogeneous catalysis[3,4] and separation sciences,[5] but also some advanced applications such as confined electron-transfer chains or quantum dots, mesoporous molecular wires, host−guest encapsulation, sensors, shape-selective polymerization, optical devices, immobilization of biomolecules, and green chemistry and environment, among others.[6]

The still growing development of functionalized mesoporous materials, combining in a single solid the structural properties of the rigid inorganic lattice with the intrinsic chemical reactivity of the organic components, has led to extending widely the scope of applications of ordered mesoporous systems.[6b,7−9] Two major families of organic−inorganic hybrids can be distinguished: class I corresponds to materials with weak bonding between organic and inorganic phases, while class II corresponds to materials where both phases are chemically grafted.[10] The latter are very attractive since the nonhydrolyzable character of the Si−C bond prevents leaching of organic groups out of materials when used in solution. Functionalization can be achieved by postgrafting of as-synthesized ordered materials[8] or directly by co-condensation of a tetra-alkoxysilane and one (or more) organoalkoxysilane(s) in the presence of a surfactant template,[9] leading to more uniform composition of the mesostructure.[11]

Most of the properties of these new high-technology materials are dependent on their structural and chemical composition as well as on the dynamical properties inside the blends. Particular reactivity can be tuned by appropriate choice of the organic functions, at least if they keep their activity upon immobilization and remain accessible to external reactants. Interest of ordered mesoporous organosilicas with this respect has been evidenced in several applied fields: high catalytic activity and selectivity,[3,4,8e,12] improved removal of toxic heavy metal species, radionuclides, or organic solvents from aqueous effluents,[12d,13−15] enhanced activity of entrapped organometallic complexes or biomolecules,[16] and thin films and sensor devices[6g,17] with better sensitivity, as compared to corresponding amorphous materials.

Accessibility to organic groups grafted within mesoporous silicas was largely studied for Hg^{II} binding to thiol-functionalized solids, which were obtained either by postsynthesis grafting[13a−d,f−i] or by the co-condensation route.[12d,13e,k,m−r] Most works have been carried out by the groups of Pinnavaia, Mercier, and Liu.[13] These ordered hybrids gave rise to better accessibility (up to 100% of binding sites filled with Hg^{II}) than those observed with using amorphous silica gels grafted with the same ligands,[13b] even if the resort to open amor-

(4) (a) Brunel, D.; Cauvel, A.; Fajula, F.; DiRenzo, F. *Stud. Surf. Sci. Catal.* **1995**, *97*, 173. (b) Fajula, F.; Brunel, D. *Microporous Mesoporous Mater.* **2001**, *48*, 119. (c) Brunel, D.; Blanc, A. C.; Galarneau, A.; Fajula, F. *Catal. Today* **2002**, *73*, 139.

(5) (a) Linden, M.; Schacht, S.; Schüth, F.; Steel, A.; Unger, K. K. *J. Porous Mater.* **1998**, *5*, 177. (b) Inagaki, S.; Ogata, S.; Goto, Y.; Fukushima, Y. *Stud. Surf. Sci. Catal.* **1998**, *117*, 65. (c) Liu, J.; Fryxell, G. E.; Mattigod, S.; Zemanian, T. S.; Shin, Y.; Wang, L.-Q. *Stud. Surf. Sci. Catal.* **2000**, *129*, 729. (d) Kisler, J. M.; Dahler, A.; Stevens, G. W.; O'Connor, A. J. *Microporous Mesoporous Mater.* **2001**, *44*−*45*, 769.

(6) (a) Vartuli, J. C.; Shih, S. S.; Kresge, C. T.; Beck, J. S. *Stud. Surf. Sci. Catal.* **1998**, *117*, 13. (b) Ozin, G. A.; Chomski, E.; Khushalani, D.; Maclachlan, M. J. *Curr. Opin. Colloid Interface Sci.* **1998**, *3*, 181. (c) Cooper, C.; Burch, R. *Water Res.* **1999**, *33*, 3689. (d) Fryxell, G. E.; Liu, J.; Mattigod, S. V.; Wang, L. Q.; Gong, M.; Hauser, T. A.; Lin, Yuehe; Ferris, K. F.; Feng, X. *Ceram. Trans.* **2000**, *107*, 29. (e) Scott, B. J.; Wirnsberger, G.; Stucky, G. D. *Chem. Mater.* **2001**, *13*, 3140. (f) Walcarius, A. *Chem. Mater.* **2001**, *13*, 3351. (g) Sakamoto, J.; Dong, W.; Dunn, B. *Proc. Electrochem. Soc.* **2001**, *2000-36*, 197. (h) Yan, A.-X.; Li, X.-W.; Ye, Y.-H. *Appl. Biochem. Biotechnol.* **2002**, *101*, 113. (i) Clark, J. H. *Acc. Chem. Res.* **2002**, *35*, 791.

(7) (a) Moller, K.; Bein, T. *Chem. Mater.* **1998**, *10*, 2950. (b) Maschmeyer, T. *Curr. Opin. Solid State Mater. Sci.* **1998**, *3*, 71. (c) Stein, A.; Melde, B. J.; Schroden, R. C. *Adv. Mater.* **2000**, *12*, 1403. (d) Sayari, A.; Hamoudi, S. *Chem. Mater.* **2001**, *13*, 3151.

(8) (a) Liu, J.; Feng, X. D.; Fryxell, G. E.; Wang, L. Q.; Kim, A. Y.; Gong, M. L. *Adv. Mater.* **1998**, *10*, 161. (b) Moller, K.; Bein, T. *Stud. Surf. Sci. Catal.* **1998**, *117*, 53. (c) Brunel, D. *Microporous Mesoporous Mater.* **1999**, *27*, 329. (d) Impens, N. R. E. N.; Van der Voort, P.; Vansant, E. F. *Microporous Mesoporous Mater.* **1999**, *28*, 217. (e) Clark, J. H.; Macquarrie, D. J.; Wilson, K. *Stud. Surf. Sci. Catal.* **2000**, *129*, 251.

(9) (a) Burkett, S. L.; Sims, S. D.; Mann, S. *Chem. Commun.* **1996**, 1367. (b) Macquarrie, D. J. *Chem. Commun.* **1996**, 1961. (c) Fowler, C. E.; Mann, S.; Lebeau, B. *Chem. Commun.* **1998**, 1825. (d) Asefa, T.; Yoshina-Ishii, C.; MacLachlan, M. J.; Ozin, G. A. *J. Mater. Chem.* **2000**, *10*, 1751. (e) Burleigh, M. C.; Markowitz, M. A.; Spector, M. S.; Gaber, B. P. *J. Phys. Chem. B* **2001**, *105*, 9935.

(10) (a) Sanchez, C.; Ribot, F. *New J. Chem.* **1994**, *18*, 1007. (b) Judeinstein, P.; Sanchez, C. *J. Mater. Chem.* **1996**, *6*, 511. (c) Sanchez, C.; Ribot, F.; Lebeau, B. *J. Mater. Chem.* **1999**, *9*, 35. (d) Sanchez, C.; Lebeau, B.; Ribot, F.; In, M. *J. Sol*−*Gel Sci. Technol.* **2000**, *19*, 31.

(11) Lim, M. H.; Stein, A.*Chem. Mater.* **1999**, *11*, 3285.

(12) (a) Maschmeyer, T.; Oldroyd, R. D.; Sankar, G.; Thomas, J. M.; Shannon, I. J.; Klepetko, J. A.; Masters, A. F.; Beattie, J. K.; Catlow, C. R. A. *Angew. Chem., Int. Ed. Engl.* **1997**, *36*, 1639. (b) Sheppard, E. W.; Zhou, W.; Maschmeyer, T.; Matters, J. M.; Roper, C. L.; Parsons, S.; Johnson, B. F. G.; Duer, M. J. *Angew. Chem., Int. Ed.* **1998**, *37*, 2719. (c) Pinnavaia, T. J.; Zhang, W. *Stud. Surf. Sci. Catal.* **1998**, *117*, 23. (d) Lim, M. H.; Blanford, C. F.; Stein, A. *Chem. Mater.* **1998**, *10*, 467. (e) Bellocq, N.; Abramson, S.; Lasperas, M.; Brunel, D.; Moreau, P. *Tetrahedron: Asymm.* **1999**, *10*, 3229. (f) Price, P. M.; Clark, J. H.; Macquarrie, D. J. *Dalton* **2000**, 101.

(13) (a) Feng, X.; Fryxell, G. E.; Wang, L.-Q.; Kim, A. Y.; Liu, J.; Kemmer, K. M. *Science* **1997**, *276*, 923. (b) Mercier, L.; Pinnavaia, T. J. *Adv. Mater.* **1997**, *9*, 500. (c) Mercier, L.; Pinnavaia, T. J. *Environ. Sci. Technol.* **1998**, *32*, 2749. (d) Liu, J.; Feng, X.; Fryxell, G. E.; Wang, L.-Q.; Kim, A. Y.; Gong, M. *Adv. Mater.* **1998**, *10*, 161. (e) Brown, J.; Mercier, L.; Pinnavaia, T. J. *Chem. Commun.* **1999**, 69. (f) Chen, X.; Feng, X.; Liu, J.; Fryxell, G. E.; Gong, M. *Sep. Sci. Technol.* **1999**, *34*, 1121 (g) Mattigod, S. V.; Feng, X.; Fryxell, G. E.; Liu, J.; Gong, M. *Sep. Sci. Technol.* **1999**, *34*, 2329. (h) Fryxell, G. E.; Liu, J.; Hauser, T. A.; Nie, Z.; Ferris, K. F.; Mattigod, S.; Gong, M.; Hallen, R. T. *Chem. Mater.* **1999**, *11*, 2148. (i) Mattigod, S. V.; Fryxell, G. E.; Feng, X.; Liu, J. In *Metal Separation Technologies Beyond 2000: Integrating Novel Chemistry with Processing*; Liddell, K. C., Ed.; Minerals, Metals & Materials Society: Warrendale, PA, 1999; pp 71−79. (j) Mercier, L.; Pinnavaia, T. J. *NATO Sci. Ser., Ser. E* **1999**, *362*, 33. (k) Brown, J.; Richer, R.; Mercier, L. *Microporous Mesoporous Mater.* **2000**, *37*, 41. (l) Fryxell, G. E.; Liu, J.; Mattigod, S. V.; Wang, L. Q.; Gong, M.; Hauser, T. A.; Lin, Y.; Ferris, K. F.; Feng, X. *Ceram. Trans.* **2000**, *107*, 29. (m) Seneviratne, J.; Cox, J. A. *Talanta* **2000**, *52*, 801. (n) Liu, A. M.; Hidajat, K.; Kawi, S.; Zhao, D. Y. *Chem. Commun.* **2000**, 1145. (o) Lee, B.; Kim, Y.; Lee, H.; Yi, J. *Microporous Mesoporous Mater.* **2001**, *50*, 77. (p) Bibby, A.; Mercier, L. *Chem. Mater.* **2002**, *14*, 1591. (q) Etienne, M.; Lebeau, B.; Walcarius A. *New J. Chem.* **2002**, *26*, 384. (r) Etienne, M.; Sayen, S.; Lebeau, B.; Walcarius A. *Stud. Surf. Sci. Catal.* **2002**, *141*, 615.

(14) (a) Feng, X.; Rao, L.; Mohs, T. R.; Xu, J.; Xia, Y.; Fryxell, G. E.; Liu, J.; Raymond, K. N. *Ceram. Trans.* **1999**, *93*, 35. (b) Ju, Y. H.; Webb, O. F.; Dai, S.; Lin, J. S.; Barnes, C. E. *Ind. Eng. Chem. Res.* **2000**, *39*, 550. (c) Lin, Y.; Fryxell, G. E.; Wu, H.; Engelhard, M. *Environ. Sci. Technol.* **2001**, *35*, 3962.

(15) (a) Beck, J. S.; Calabro, D. C.; McCullen, S. B.; Pelrine, B. P.; Schmitt, K. D.; Vartuli, J. C. U.S. Patent 5,220,101, Mobil Oil Corporation, USA, 1993. (b) Zhao, X. S.; Lu, G. Q. *J. Phys. Chem. B* **1998**, *102*, 1556. (c) Huq, R.; Mercier, L.; Kooyman, P. J. *Chem. Mater.* **2001**, *13*, 4512.

(16) See, e.g., (a) Maschmeyer, T.; Thomas, J. M.; Masters, A. F. *NATO ASI Ser., Ser. C* **1997**, *498*, 461. (b)Leventis, N.; Elder, I. A.; Rolison, D. R.; Anderson, M. L.; Merzbacher, C. I. *Chem. Mater.* **1999**, *11*, 2837. (c) Xu, J.; Feng, Q.; Dong, H.; Wei, Y. *Polym. Prepr. (Am. Chem. Soc., Div. Polym. Chem.)* **2000**, *41*, 1046. (d) Yan, A.-X.; Li, X.-W.; Ye, Y.-H. *Appl. Biochem. Biotechnol.* **2002**, *101*, 113.

(17) See, e.g., (a) Lu, Y.; Ganguli, R.; Drewien, C. A.; Anderson, M. T.; Brinker, C. J.; Gong, W.; Guo, Y.; Soyez, H.; Dunn, B.; Huang, M. H.; Zink, J. I. *Nature* **1997**, *389*, 364. (b) Gimon-Kinsel, M. E.; Balkus, K. J., Jr. *Stud. Surf. Sci. Catal.* **1998**, *117*, 111. (c) Anderson, M. L.; Rolison, D. R.; Merzbacher, C. I. *Proc. SPIE Int. Soc. Opt. Eng.* **1999**, *3790*, 38. (d) Sayen, S.; Etienne, M.; Bessière, J.; Walcarius A. *Electroanalysis* **2002**, *14*, 1521.

phous solids displaying large pores (>60 Å) enabled reaching accessibility as high as 90%.[18] Accessibility to active centers is also crucial in heterogeneous catalysis, for which the interest of ordered mesoporous silicas has been pointed out.[8e,11,12b,c,19,20]

In addition to accessibility, the speed at which reactants are allowed to reach active centers in the mesoporous material is also an important parameter affecting its performance. This is especially critical when reactions are strongly diffusion-controlled, for example, solid−liquid extraction[13] or electrochemical sensing,[6g,17d,21,22] for which the effective rate is expected to be higher in organized porous structures than in nonfractal particles.[23] Although reaction speeds were scarcely considered in the literature,[13c,d,o,r,20b] detailed studies of diffusion-controlled reactions in mesoporous organosilicas are not widespread.[13g,p] This was essentially applied to the accumulation of Hg^{II} species by self-assembled mercaptan on mesoporous silica[13g] and in thiol-functionalized mesoporous silica microspheres prepared according to the co-condensation route.[13p] Mattigod et al.[13g] described a rather fast binding of complexed mercury(II) (HgI_4^{2-}) on a thiol-grafted mesoporous material displaying 5-nm pore size, a surface area of 871 $m^2\ g^{-1}$, and particle size ranging between 5 and 15 μm: 80−95% completion was achieved in 5 min. In a more detailed approach, Bibby and Mercier[13p] have characterized the uptake kinetics of Hg^{II} in thiol-containing silica microspheres of approximately 12-μm size but displaying smaller pore diameters (24−32 Å) and surface areas ranging from about 1000 to 1260 $m^2\ g^{-1}$; having applied the shrinking core model,[24] they calculated diffusion coefficients in the range 10^{-11}−10^{-10} $cm^2\ s^{-1}$ at the equilibrium. Surprisingly, this model led to diffusion coefficients increasing with increasing Hg^{II} loading in the material, which brought the authors to propose an ion permeation-displacement mechanism to explain their observation.

In a previous report,[18] we provided an experimental approach for studying diffusion of protons, Hg^{II} and Cu^{II}, in amorphous silica gels grafted with either amine or thiol groups. It was shown notably that both protonation of silica gels bearing amine ligands, and binding of metallic species on these organically modified amorphous silicas, were dependent on pore size of the material and size of the reactant, on density of grafted organic sites, and on the nature of the starting material. The present paper aims at characterizing physical diffusion in various ordered mesoporous silicas grafted with the same ligands. In particular, we examine the influence of structure and porosity of five mesostructured silicas, grafted with various amounts of NH_2 or SH groups, on the access rates of H^+, Hg^{II}, and Cu^{II} to the binding sites. Efforts are concentrated on monitoring reaction rates at the early times of the experiments due to the usually fast diffusion kinetics. Modelization is applied to estimate the apparent diffusion coefficients. A comparison is made with previous results obtained with corresponding amorphous solids.

Table 1. Physicochemical Characteristics of Starting Mesoporous Materials.

	nitrogen adsorption			
sample	BET surface area ($m^2\ g^{-1}$)	total pore volume ($cm^3\ g^{-1}$)	pore diameter[a] (Å)	average particle size[b] (μm)
MCM-41(A)	1045	0.98	38	40
MCM-41(B)	1038	0.89	34	15−120[c]
MCM-41(C)	848	1.56	73	32
SBA-15	644	1.05	65	58
MCM-48	1030	0.94	37	57

[a] Estimated according to $D = (4V_p/A)$, with D = average pore diameter, V_p = total pore volume, and A = specific surface area, according to ref 40. [b] Based on number, determined from cumulative particle size distribution analysis. [c] Bimodal distribution (median = 77 μm).

2. Experimental Section

2.1. Reagents, Solutions, and Materials. All reagents were analytical-grade and solutions were prepared either with high-purity water (18 MΩ-cm) from a Millipore Milli-Q water purification system or as 95:5 ethanol:water mixtures (Merck). Metal ion solutions were obtained from their nitrate salts ($Hg(NO_3)_2$ [**Attention! Mercury is highly toxic**] or $Cu(NO_3)_2$, purchased from Prolabo) and their concentration was checked using the corresponding standards (Titrinorm). Various acids were used (hydrochloric min. 36%, trifluoroacetic min. 98%, and picric, from Fluka or Prolabo); they were standardized using 1.002 M sodium hydroxide (Titrinorm, Prolabo).

Five different micelle-templated mesoporous silica (MTS) samples were used for this study: two MCM-41 types of small-pore size (about 30−35 Å), two hexagonal structures of larger pore size (about 60−70 Å), and one MCM-48 type of small-pore size (about 35 Å). They have been codified as follows: MCM-41(A), MCM-41(B), MCM-41(C), SBA-15,[2f] and MCM-48 (Table 1). MCM-41(A) and MCM-41(B) display an architecture with small pores. MCM-41(B) was gratefully donated by M. Hudson and prepared according to a published procedure[25] (that leading to heterogeneous particle morphology, not to the homogeneous spheres, in ref 25). MCM-41(A) synthesis was performed from two starting solutions: (a) 500 mL of H_2O containing 24.5 g of cetyltrimethylammonium bromide (CTAB, dissolution at 35 °C) and (b) 75 g of H_2O + 75 g of sodium silicate solution (SiO_2 27%, NaOH 14%, from Fluka). These solutions, a and b, were then mixed together under strong stirring. The pH was then decreased to 8 by adding 210 mL of HCl (1 M) within 5 min. A white precipitate was observed at about pH 12. The resulting solid is filtered on Buchner, washed with water, and dried at 60 °C. MCM-41(C) and SBA-15 have larger pores. MCM-41(C) was prepared according to the same protocol as that applied to produce the MCM-41(A) sample,

(18) Walcarius, A.; Etienne, M.; Bessière, J. *Chem. Mater.* **2002**, *14*, 2757.
(19) Pinnavaia, T. J.; Pauly, T. R.; Kim, S. S. *Spec. Publ.—R. Soc. Chem.* **2001**, *266*, 19.
(20) (a) Maschmeyer, T.; Rey, F.; Sankar, G.; Thomas, J. M. *Nature* **1995**, *378*, 159. (b) Macquarrie, D. J.; Jackson, D. B. *Chem. Commun.* **1997**, 1781. (c) Bossaert, W.; De Vos, D. E.; Van Rhijn, W. M.; Bullen, J.; Grobet, P. J.; Jacobs, P. A. *J. Catal.* **1999**, *182*, 156.
(21) (a) Walcarius, A. *Electroanalysis* **1998**, *10*, 1217. (b) Walcarius, A.; Despas, C.; Trens, P.; Hudson, M. J.; Bessière, J. *J. Electroanal. Chem.* **1998**, 453, 249. (c) Walcarius, A.; Lüthi, N., Blin, J.-L.; Su, B.-L.; Lamberts, L. *Electrochim. Acta* **1999**, *44*, 4601. (d) Walcarius, A.; Bessière, J. *Chem. Mater.* **1999**, *11*, 3009. (e) Walcarius, A. *Electroanalysis* **2001**, *13*, 701. (f) Etienne, M.; Bessière, J.; Walcarius, A. *Sens. Actuators B* **2001**, *76*, 531.
(22) (a) Villemure, G.; Pinnavaia, T. J. *Chem. Mater.* **1999**, *11*, 789. (b) Innocenzi, P.; Martucci, A.; Guglielmi, M.; Bearzotti, A.; Traversa, E. *Sens. Actuators B* **2001**, *76*, 299.
(23) (a) Coppens, M.-O.; Froment, G. F. In *Fractals and Chaos in Chemical Engineering*, Proceedings of the International CFIC 96 Conference, Rome, Sept 2−5, 1996; Giona, M., Biardi, G., Eds.; World Scientific: Singapore, 1997; pp 15−26. (b) Kaerger, J.; Freude, D. *Chem. Ing. Techn.* **2001**, *73*, 1517.
(24) Ruthven, D. M.; Kärger, J. *Diffusion in Zeolites*; Wiley-Interscience: New York, 1992; pp 250−255.
(25) (a) Unger, K. K. *Adv. Chem. Ser.* **1994**, *234*, 165. (b) Grun, M.; Unger, K. K.; Matsumoto, A.; Tsutsumi, K. *Microporous Mesoporous Mater.* **1999**, *27*, 207.

except that 1,3,5-trimethylbenzene (TMB) was added in the surfactant solution in a TMB/CTAB ratio equal to 13. The SBA-15 sample was prepared by dissolving a 8-g aliquot of the triblock copolymer $EO_{30}PO_{70}EO_{30}$ (Pluronic P123) in 250 mL of aqueous solution containing 1.9 M HCl, at about 38 °C, under stirring for 1−2 h. Tetraethoxysilane (TEOS, 15.95 mL) was then added to this mixture, which was allowed to react in a polypropylene flask for 24 h at 38 °C and then 2 days at 90 °C. The resulting white solid was filtered on Buchner, washed with water, and dried at 60 °C. Finally, the cubic MCM-48 structure was obtained as follows: 96.8 g of H_2O + 50 mL of ethanol + 2.4 g of CTAB were mixed under constant stirring for 5 min. Afterward, 13.6 mL of ammonia (28% NH_3 in water, Fluka) was added under stirring, which was maintained for 10 min, and then 3.4 g of TEOS was introduced into the vessel while keeping constant stirring for 5 min more. The reactive medium was then placed for 17 h at 70 °C in a stoppered polypropylene flask. The final product was filtered on Buchner, washed with water, and dried at 70 °C. For all products, the template was removed by calcination at 540 °C for 4 h (with both an increase and decrease in temperature carried out progressively within 4 h). For sake of comparison, a commercially available silica gel (SI60 from Geduran) was also used.

2.2. Chemical Modification of Mesoporous Silica Samples. Grafting amine or thiol groups on the walls of MTS samples was performed in dry toluene (99%, Merck) by reaction with 3-aminopropyltriethoxysilane (APTES, 99%, Sigma-Aldrich) or mercaptopropyltrimethoxysilane (MPTMS, 95%, Lancaster), according to a similar procedure as that applied for grafting silica gels.[18,26] Briefly, 250 mg of each MTS sample was suspended in 25 mL of toluene, stirred a few minutes at room temperature, and allowed to react under refluxing with the organosilane (2 mL of APTES or 1 mL of MPTMS), which was slowly added to the mixture. Most solids were dried (at 120 °C for 2 h) to remove most water molecules prior to grafting, except for MCM-41(A) sample in which trace water was intentionally kept present to allow some hierarchical polymerization of the grafting agent within the pores of the material. After reaction (for 2 h for APTES and 24 h for MPTMS), the mixtures were cooled to room temperature and the solids filtered, washed with toluene, and dried under reduced pressure for 24 h. The grafted materials were named afterward by using a prefix, APS (aminopropylsilica) or MPS (mercaptopropylsilica), followed by the type of MTS (MCM-41(A), MCM-41(B), MCM-41(C), SBA-15, or MCM-48). They were characterized by various physicochemical techniques (N_2 adsorption/desorption, X-ray diffraction (XRD), granulometry); in particular, it was checked that no significant loss in crystallinity was observed after grafting. For all samples, the amount of grafted organic functions was determined from elemental analyses performed at the "Service Central d'Analyse" (CNRS, Lyon).

2.3. Instrumentation. The maximum capacity of materials for reaction with protons and copper(II) species (APS samples) or with mercury(II) species (MPS samples) was determined after 24 h of reaction in a medium containing the reactant in excess, by solution phase analysis of the remaining reactant concentration. The extent of protonation was followed by pH monitoring (calibrated glass electrode associated to a model 691 pH meter, from Metrohm) and/or via the disappearance of the associated anion, as measured by capillary electrophoresis with the aid of a capillary ion analyzer equipped with a negative high-voltage power supply (Waters, CIA) and a bare fused silica capillary (length, 60 cm; diameter, 75 μm). Quantitative analysis of copper(II) and mercury(II) in solution was carried out by inductively coupled plasma-atomic emission spectroscopy (ICP-AES, Plasma 2000, Perkin-Elmer).

Measurement of specific surface area, pore volume, and estimation of pore size of materials were achieved by recording nitrogen adsorption−desorption isotherms, at 77 K in the relative pressure range from about 10^{-5} to 0.99, on a Coulter instrument (model SA 3100). Particle size distribution was measured with use of a light-scattering analyzer (model LA920, Horiba), based on the Mie scattering theory. Scanning electron microscopy (SEM) was performed with a Philips XL30 apparatus. Crystallinity of materials was checked by X-ray diffraction (XRD), which was carried out using a classical powder diffractometer with transmission geometry, equipped with a Mo tube (quartz monochromator, $K\alpha_1$ radiation, λ = 0.070930 nm) and a scintillation counter.

2.4. Procedures. *2.4.1. Kinetic Experiments: Protonation of Aminopropyl-Grafted Solids.* Kinetic experiments involving the protonation of APS samples have been carried out in batch conditions, according to our previously described procedure.[18] Briefly, an accurate amount of protons was added rapidly to a suspension containing a homogeneous dispersion of APS particles in a liquid phase (water or ethanol) and pH was monitored continuously under constant stirring, to measure the consumption of protons as time elapsed. Data measurement was performed after appropriate calibration,[18] at a frequency of 4 Hz, by applying homemade software connected to the Metrohm 691 pH-meter (with glass electrode Metrohm No. 6.0222.100). Standard deviation is expected to be less than 5%.

2.4.2. Kinetic Experiments: Adsorption of Mercury(II) on Mercaptopropyl-Grafted Solids and Copper(II) on Aminopropyl-Grafted Materials. Preliminary batch experiments with intermittent concentration measurements have rapidly indicated that the uptake rates of metal species by mesoporous solids were very fast (typically more than 50% reaction in less than 1 min) so that the discontinuous analysis of remaining Hg^{II} or Cu^{II} in solution (which had been successfully applied to study the diffusion rates within amorphous materials)[18] was prevented here. A new electrochemical method was then developed and applied to the continuous monitoring of solution-phase Hg^{II} or Cu^{II} in MPS or APS suspensions. It involves the use of a rotating disk electrode in conditions where steady-state currents are directly proportional to the analyte concentration. A typical experiment for Hg^{II} can be described as follows. A vitreous carbon electrode is immersed into a deaerated (N_2 purge) 200-mL solution containing the metal species at an initial concentration of 2.0×10^{-4} M and 0.1 M HNO_3 and allowed to rotate at the speed of 2000 rd min^{-1}. A constant potential of −0.5 V (vs SCE) is then applied to the rotating electrode awaiting for a constant current, which is typically obtained after 5−10 min. At this stage, the electrode response is proportional to the Hg^{II} concentration in the 2×10^{-6} to 2×10^{-4} M range, as ascertained by appropriate calibration. While the constant potential of −0.5 V applied to the rotating electrode is being maintained, a selected amount of solid material (e.g. MPS) is then added into the cell, after being previously dispersed in 5-mL aliquot of water under sonication to ensure the fastest dispersion of particles in the measurement cell, as possible, to obtain a steady-state distribution of particle size in the voltammetric cell; this was completed in less than 1 s and remained macroscopically unchanged during the adsorption experiments. The steady-state current recorded at the rotating disk decreased as a result of Hg^{II} consumption by the MPS material. Metal uptake was calculated by the difference between the measured transient concentrations of Hg^{II} in solution (one current sampling every each half-second) and the starting concentration value. After equilibrium was reached, the final metal concentration was also determined by anodic stripping differential pulse voltammetry on gold electrode (Hg^{II}) or ICP-AES (Cu^{II}) to check the long-term stability of the continuous electrochemical monitoring. All electrochemical experiments have been performed with using a Model 283 potentiostat/galvanostat EG&G Princeton Applied Research (PAR), monitored by the M270 electrochemical research software (EG&G PAR). They were carried out at room temperature in an undivided three-electrode with the aid of rotating disk electrodes (vitreous carbon or gold). The counter electrode was made of a platinum wire, and a saturated calomel electrode

(26) Vansant, E. F.; Van der Voort, P.; Vrancken, K. C. *Characterisation and Chemical Modification of the Silica Surface*; Elsevier: Dordrecht, The Netherlands, 1995.

Table 2. Physicochemical Characteristics of Mesoporous Silicas Grafted with Either Aminopropyl or Mercaptopropyl Groups

	nitrogen adsorption			amount of grafted ligands[a]		average particle size[b]	
sample	BET surface area ($m^2\ g^{-1}$)	total pore volume ($cm^3\ g^{-1}$)	pore volume loss after grafting (%)	aminopropyl (mmol g^{-1})	mercaptopropyl (mmol g^{-1})	based on number (μm)	based on volume (μm)
APS−MCM-41(A)	87	0.16	84	3.3		22[c]	95[c]
APS−MCM-41(B)	428	0.24	73	2.8		12[c]	55[c]
APS−MCM-41(C)	411	0.76	51	2.6		17[c]	39[c]
APS−SBA-15	357	0.73	30	2.2		11	47
APS−MCM-48	662	0.31	67	3.0		14	84
MPS−MCM-41(A)	162	0.19	81		2.8	16	29
MPS−MCM-41(B)	818	0.52	42		1.55	8	15
MPS−MCM-41(C)	706	1.24	20		1.0	12	17
MPS−SBA-15	467	0.79	25		1.0	6	22
MPS−MCM-48	390	0.23	75		2.7	9	18

[a] Expressed per gram of grafted material. [b] Determined from cumulative particle size distribution analysis. [c] Measured after about 2 days of aging in atmosphere (i.e., liable to have undergone some damage).

(SCE) served as reference. Particle size distributions were measured in the same conditions as those applied for kinetic experiments, that is, after ultrasonic treatment and equilibration in the solution.

2.4.3. Kinetic Data Presentation and Treatment. All data resulting from kinetic experiments are presented in the form of plots giving the evolution of Q/Q_0 ratios versus time, where Q is the amount of reactant (analyte) that has reached the binding sites within/on the solid particles at time t and Q_0 is either the theoretical maximum of binding sites (that is, the total amount of grafted ligands in the material) or the maximum of accessible binding sites for the target analyte species (that is, the amount of analyte within/on the solid at time $= \infty$). Q/Q_0 is therefore equal to zero at $t = 0$ and can reach unity after completion of the reaction in case of 100% accessibility; otherwise, the equilibrium Q/Q_0 values observed at time $= \infty$ is a measurement of the degree of accessibility of the binding sites to the target analyte. Variation of Q/Q_0 with time constitutes a direct indication of the binding rate of the analyte species to the organic ligands grafted to the various mesoporous structures (acids or Cu^{II} on APS and Hg^{II} on MPS samples).

The rate-determining step of binding processes is expected to be the physical diffusion of the analytes inside the organically modified porous structures (eventually with their associated counterions). Two main parameters are affecting this kind of mass-transfer reaction: the particle size (and shape) and the apparent diffusion coefficient of the analyte inside the particle. The average particle size (based on volume) can be easily calculated from measurements of particle size distribution.[18] Therefore, fitting the kinetic curves Q/Q_0 versus time by an appropriate diffusion model by using this average particle size would lead to estimation of the apparent diffusion coefficient of reactive species within the material. Choosing the model that is most appropriate for mesoporous materials is, however, not a simple task because these solids are made of regular channels of cylindrical shape and most often exist under aggregates made of several individual crystallites.[27] Consistent with our previous report on amorphous grafted silicas,[18] we have chosen in a first approximation a spherical non-steady-state diffusion model, by considering that most materials were in the form of "granules" made of randomly packed individual crystals of size much lower than that of the resulting aggregates. Of course, this model is not ideal since diffusion in a single linear channel is expected to be monodimensional (in contrast to the three-dimensional diffusion in a sphere), but this approach allows a comparison of the results presented here for all the mesoporous materials between them and to those obtained for the corresponding amorphous solids.[18] Moreover, the linear diffusion model would be valid only for single crystals of "perfect" shape on a sufficiently long scale (with a crystal length much higher than pore size and easily measurable), which is not the case for our samples. Kinetic curves were thus fitted according to the diffusion in a spherical material,[28] as given by eq 1, as established in the form of a level-headed sum of each contribution of populations displaying the same particle size a_x,

$$\frac{Q}{Q_0} = \sum_{x=1}^{x=n} f_{a_x}\left[6\left(\frac{Dt}{a_x^2}\right)^{1/2}\left\{\pi^{-1/2} + 2\sum_{n=1}^{\infty}(-1)^n \text{ ierfc}\frac{na_x}{\sqrt{Dt}}\right\} - 3\frac{Dt}{a_x^2}\right] \quad (1)$$

where Q/Q_0 has been defined above, D is the apparent diffusion coefficient, a is the particle size radius, "ierfc" is the error function, t is time, and f_{a_x} is the relative fraction of particles having the same size a_x; this fraction ranges from 0 to 1 and is determined from particle size distribution measurements.

3. Results and Discussion

3.1. Characteristics of Materials after Modification with Organic Groups. Effect of grafting on the physicochemical properties of mesoporous silica samples is summarized in Table 2. As expected from the space occupied by the organic moieties bound on the inner surface of the mesopores, both specific surface area and pore volume were found to decrease upon modification. This tendency was much more pronounced for small-pore materials and was stronger for samples containing larger amounts of grafted groups, in agreement with previous results on thiol- and amine-functionalized mesoporous silicas.[13e,29] In particular, APS−MCM-41-(A) and MPS−MCM-41(A) samples exhibit a considerable decrease of porosity as compared to the raw material, which can be explained by the rather large amount of grafted groups. In these samples, some hierarchical polymerization of the organosilane could have occurred, concurrent to the grafting process, because of the existence of some physisorbed water in the starting MCM-41(A) solid (about 3% H_2O, that is, 1.7 mmol g^{-1}, as determined by thermogravimetric analysis). This process is, however, thought to be not so significant as the water content is much lower than the final amounts of grafted groups, and because surface

(27) Sonwane, C. G.; Bhatia, S. K. *Langmuir* **1999**, *15*, 2809.

(28) Crank, J. *The Mathematics of Diffusion*; Clarendon Press: Oxford, 1975.

(29) Burleigh, M. C.; Markowitz, M. A.; Spector, M. S.; Gaber, B. P. *Chem. Mater.* **2001**, *13*, 4760.

coverage is always lower than that corresponding to the monolayer (e.g., 1.9 aminopropyl groups by nm^2, as compared to the maximum theoretical value of 2.05 groups per nm^2, according to Vrancken et al.[30]). Anyway, grafting mesoporous solids displaying small-pore size (~35 Å) resulted in great occupation of the pore volume by the organic groups (about 3.1−3.4 and 2−2.8 mmol cm^{-3}, respectively, for aminopropyl- and mercaptopropyl groups), which would affect both accessibility to the active sites and diffusion rates within the hybrid material. Pore volume occupancy in grafted solids with larger pore diameters (SBA-15 and MCM-41(C) samples) was found to be 2−3 times lower than that in small-pore solids.

It was checked by XRD measurements that the mesoporous architecture remained intact after grafting, as demonstrated by localization of the main diffraction peaks at the same *d*-spacings (e.g., typical reflections for the hexagonal SBA-15: (raw material) d_{100} = 92.7 Å, d_{110} = 54.0 Å, d_{200} = 46.9 Å; (APS−SBA-15) d_{100} = 91.9 Å, d_{110} = 53.9 Å, d_{200} = 46.8 Å; (MPS−SBA-15) d_{100} = 92.1 Å, d_{110} = 53.9 Å, d_{200} = 46.8 Å). As previously observed for the same kind of grafted silicas, however, a decrease in the intensity of diffraction peaks was observed as a consequence of partial structure collapse of the ordered phases[31] or due to contrast matching between the inorganic framework and the organic ligands.[13b] Structure collapse was especially observed with APS materials because of the basic character of amine groups, which can contribute to local hydrolysis events in the presence of water molecules. This harmful effect was enhanced when increasing the contact time between APS samples and the atmosphere as a result of extended hydration, as highlighted by further decrease in the d_{100} peaks. The first damage due to hydrolysis in materials of the M41S family is indeed a structural loss, which tends to increase when increasing pH.[32] This effect can also contribute to the lower BET surface areas usually observed after grafting amine groups on mesoporous solids in comparison to solids grafted with thiol functions (Table 2). Finally, particle size distribution was affected by the grafting process, inducing a significant decrease in the average particle size due to attrition occurring during functionalization as a consequence of mechanical stirring. This phenomenon was more important with MPS samples than with APS because of longer reaction time in the former case; this behavior was also observed with amorphous gels,[18] even if MCM-type aggregates are not of the same nature as gels.

Mesoporous silicas functionalized with mercaptopropyl ligands are often represented in the form of organic branches spatially arranged along the pore channel in a configuration perpendicular to the silica walls with thiol groups pointing at the center of the cylindrical pore.[13b,p,33] This schematic view appears to be adequate since no interaction between thiol functions

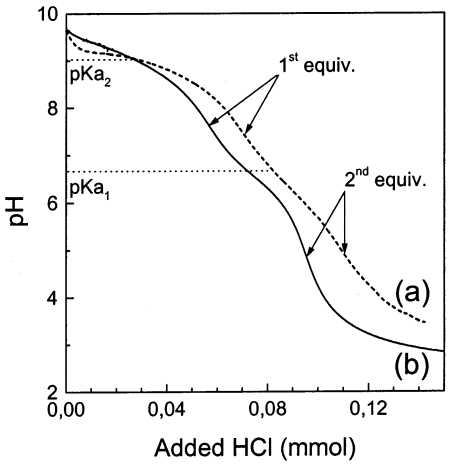

Figure 1. Titration curves for 50 mg of APS−MCM-41(B) (a) and APS−SBA-15 (b) in 50 mL of aqueous solution, obtained by adding 0.0104 M HCl at 0.03 mL min^{-1}.

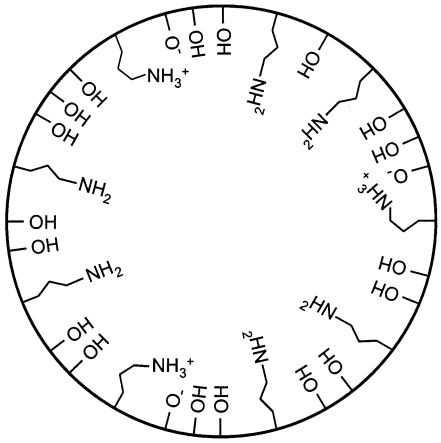

Figure 2. Schematic view depicting possible arrangement of chemical functions (silanol, propylamine, and propylammonium-silanolate groups) located inside the mesopores of APS samples.

and (residual) silanol groups is expected to occur. It could be less appropriate for APS materials because amine functions are known to interact strongly with silanol groups (i.e., via acid−base reactions[34]), which leads in the case of silica gels grafted with aminopropyl groups to the formation of zwitterion-like species ($\equiv SiO^-, {}^+H_3NC_3H_6-Si\equiv$), as evidenced by acid−base titration, IR, and XPS measurements.[18,35] Figure 1 reveals that this is also true for mesoporous silicas grafted with aminopropyl groups, as the acid−base titration curves recorded for APS−MCM-41(B) and APS−SBA-15 are characterized by two successive pH jumps corresponding to the successive protonation of "free" amine groups (pK_{a_2} close to 9) and silanolate part of the zwitterions (pK_{a_1} = 6.7). This latter is very close to the intrinsic pK_a value reported to be 6.8 for the surface silanol groups of silica.[36] According to these observed trends, a cross-sectional view of a mesopore channel of MCM-41 grafted with aminopropyl groups can be proposed as depicted in Figure 2, which represents the existence of residual silanol groups, zwiter-

(30) Vrancken, K. C.; van der Voort, P.; Possemiers, K.; Vansant, E. F. *J. Colloid Interface Sci.* **1995**, *174*, 86.
(31) Evans, J.; Zaki, A. B.; El-Sheikh, M. Y.; El-Safty, S. A. *J. Phys. Chem. B* **2000**, *104*, 10271.
(32) (a) Trong On, D.; Zaidi, S. M. J.; Kaliaguine, S. *Microporous Mesoporous Mater.* **1998**, *22*, 211. (b) Landau, M. V.; Varkey, S. P.; Herskowitz, M.; Regev, O.; Pevzner, S.; Sen, T.; Luz, Z. *Microporous Mesoporous Mater.* **1999**, *33*, 149.
(33) Mercier, L.; Pinnavaia, T. J. *Chem. Mater.* **2000**, *12*, 188.
(34) Despas C.; Walcarius, A.; Bessière, J. *Langmuir* **1999**, *15*, 3186.
(35) Zhmud, B. V.; Sonnefeld, J. *J. Non-Cryst. Solids* **1996**, *195*, 16.
(36) Schindler, P.; Kamber, H. R. *Helv. Chim. Acta* **1968**, *51*, 1781.

rion-like species made of silanolate groups interacting with propylammonium functions ($\equiv SiO^-,{}^+H_3NC_3H_6-Si\equiv$), and "free" aminopropyl moieties ($\equiv Si-C_3H_6NH_2$). Interestingly, the ratio between $\equiv SiO^-,{}^+H_3NC_3H_6-Si\equiv$ and $\equiv Si-C_3H_6NH_2$ species was always found to be about 40:60 independent of the material. SA similar ratio was also observed for amorphous silica gels grafted with the same ligand,[18] which demonstrates an equivalent surface chemistry in internal channels of amine-functionalized ordered silicas, but the driving force responsible for such a behavior remains unexplained at this stage.

3.2. Accessibility to the Binding Sites. The ability for a target reactant to reach the organic active sites grafted on the internal surfaces of mesoporous materials has been studied for protonation of APS samples and mercury(II) uptake by MPS solids.

It was reported earlier that protonation of aminopropyl-grafted silica gels can be achieved quantitatively after a sufficiently long reaction time (>5 h, to overcome mass-transfer resistance), making acid−base titration of APS a suitable method of determination of organic groups loading in such amorphous materials.[18,37] The results depicted in Figure 1 indicate that it might not be the case for ordered APS samples. Indeed, the quantities of protons that have been consumed to reach the equivalent point allowed the amounts of protonated amine groups in the materials to be calculated, which were respectively 2.2 and 1.9 mmol g^{-1} for APS−MCM-41(B) and APS−SBA-15 (titration duration was 5−6 h). These values correspond respectively to 79 and 85% of the total amounts of amine groups in each solid, as determined by elemental analysis. Confirmation of incomplete accessibility for protonation of these groups grafted in mesoporous materials was given by treating all the amine-bearing ordered solids with an excess of protons and measuring their consumption after 24 h of equilibration: reaction yields ranging from 70 to 85% were observed, with a trend to better accessibility in large-pore materials. Measurements of proton consumption as a function of time indicate very fast reaction rates at the early times of the experiment and dramatically slow ones after obtaining protonation of about 40% of the total capacity of the material (see Figure 3 for APS−MCM-48 as an example). Such breakthrough in the kinetic curves is much more steep than that reported for the corresponding amorphous solids.[18] One hypothesis that can be proposed to explain, at least in part, the noncompletion of reactions is the progressive pore filling upon protonation (and charge balance with the counteranion, Cl^- in this case) and therefore the lack of place for reaching further the amine functions located deeper in the mesopores, far away from the pore entrance. Indeed, nitrogen adsorption experiments performed on APS samples after 24 h of reaction with an excess of HCl have revealed some blocking of pores in materials made of narrow apertures (with specific surface areas lower than 40 $m^2\ g^{-1}$ for APS−MCM-41-(A) and APS−MCM-41(B)). But this cannot be the unique explanation as the materials characterized by large-pore systems were found to retain rather high porosity after undergoing the same treatment with excess HCl (specific surface areas remaining as high as 340 $m^2\ g^{-1}$ for APS−SBA-15 and APS−MCM-41(C)). Further discussion and tentative explanation will be given later on, when mass-transfer rates associated with protonation of APS materials are characterized (see section 3.4.).

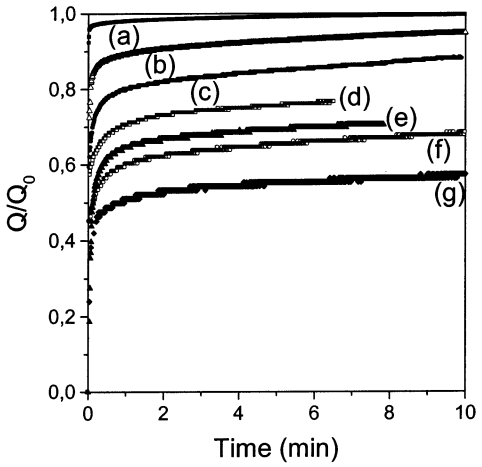

Figure 3. Protonation kinetics for APS−MCM-48 (10 mg) in 25 mL HCl solutions. The initial concentration of protons was adjusted to obtain various $H^+/R-NH_2$ ratios: (a) 15%; (b) 30%; (c) 50%; (d) 65%; (e) 72%; (f) 80%; (g) 100%. $Q_0 = 1$ is defined with respect to the initial amount of protons (that is, the maximum amount of $R-NH_2$ groups that can be protonated), while Q is the amount of protonated $R-NH_2$ groups ($R-NH_3^+\ Cl^-$).

Adsorption of mercury(II) species on thiol-functionalized mesostructures, obtained either by postsynthesis grafting or via the co-condensation route, was largely studied to highlight the advantages of uniform pore structures in the design of adsorbents with high capacities.[13a−c,e,k,p,r] Brown et al.[13k] have given a survey of the data available up to the year 2000, from which they drew a general (though not absolute) outcome showing that the adsorbents should have channel diameters in the mesopore range to allow 100% accessibility to all the binding sites.

Adsorption results obtained with the five mesoporous silicas grafted with mercaptopropyl groups investigated here are summarized in Table 3. In the MCM-41 series, the large-pore systems (MPS−SBA-15 and MPS−MCM-41(C)) gave rise to 100% accessibility as all thiol groups can be attained by an equivalent amount of Hg^{II} species (in the form of Hg^{2+} as experiments have been performed in 0.1 M HNO_3), agreeing with previous conclusions.[13k] By comparison, amorphous silica gels grafted with the same ligands and displaying approximately the same pore sizes (≈55−65 Å) gave rise to incomplete complexation (87−90%),[18] confirming further the advantages of the regular structure. Getting such Hg/S molar ratio equal to unity also indicates that all thiol groups remain active upon grafting and that no oxidation into noncomplexant disulfide groups could have occurred. No pore blocking was noticed and mesoporosity was kept after mercury binding.

In contrast, less-than-complete complexation was observed with the small-pore MCM-41 structures (MPS−MCM-41(A) and MPS−MCM-41(B)), and limitation was especially outstanding for the MPS−MCM-41(A) sample (only 29% access) where some hierarchical polymerization had been allowed. Mercaptopropyl groups were less

(37) Yang, J. J.; El-Nahhal, I. M.; Chuang, I.-S.; Maciel, G. E. *J. Non-Cryst. Solids* **1997**, *209*, 19.

Table 3. Physicochemical Characteristics of Mercaptopropyl-Grafted Mesoporous Materials after 24 h of Equilibration with an Aqueous Solution Containing Hg^{II} Excess

			nitrogen adsorption after Hg^{II} binding		
sample	extent of Hg^{II} uptake[a] (mmol g^{-1})	accessible SH groups[b] (%)	BET surface area (m^2 g^{-1})	total pore volume (cm^3 g^{-1})	pore volume loss after reaction[c] (%)
MPS−MCM-41(A)	0.8	29	26	0.06	70
MPS−MCM-41(B)	1.4	90	554	0.32	39
MPS−MCM-41(C)	1.0	100	536	0.86	31
MPS−SBA-15	1.0	100	326	0.58	27
MPS−MCM-48	1.4[5]	54	18	0.05	88

[a] Calculated by mass of the starting material. [b] Based on the number of mercaptopropyl groups grafted on the material (hypothesis of 1:1 complex, as suggested earlier; see ref 13). [c] Calculated with respect to the pore volumes of starting MPS materials.

numerous and more sparsely distributed in the MPS−MCM-41(B) material, and exclusively located on the channel walls, so that a great part of them (90%) were available for complexation due to favorable spatial distribution of reactive sites. This ordered solid displays mesopores of about 25 Å in diameter; to obtain the same performance with use of corresponding amorphous adsorbents, in terms of access to the active sites, they must possess an average pore size more than 2 times larger.[18] An interesting case is that of the cubic MPS−MCM-48 structure for which the ungrafted material was characterized by similar pore size as that of the MCM-41(B) sample (Table 1). Due to a higher silanol population, grafting MCM-48 led to an amount of ligands superseding by 1.75-fold that contained in MPS−MCM-41(B) (Table 2). This induced significant restriction of total pore volume and only 54% of thiol groups were accessible for complexation with Hg^{II} species; after metal adsorption, the material was microporous with a pore system nearly blocked (Table 3). In contrast, the solid-phase complexants exhibiting substantially superior metal-binding properties retained rather high specific surface areas and total pore volumes upon metal complexation (Table 3).

Mesopore size and density of active sites are the two main parameters affecting the accessibility of thiol groups to mercury ion binding in thiol-grafted ordered mesoporous silicas. As already stated,[13k] adsorbents with channel diameters in the mesopore range (down to 20 Å) allow total access to the binding sites, while further decrease in porosity results in uncompleted complexation. Also, increasing the ligand density in the material leads to inferior Hg^{II} binding properties. For grafted solids, these two parameters are linked between them as larger amounts of ligands would occupy more space in the mesoporous structure. Even when effort is made to confine a large amount of mercaptopropyl groups as functional monolayers on the internal walls of mesoporous silica, uncompleted accessibility was observed.[13a] Such limitation is probably due to steric hindrance but could also be due to partial formation of uncomplexant disulfide groups, which might be intensified at high thiol contents (increased closeness). A promising avenue for enhancing the active sites density while maintaining pore size in the mesoporous range is the one-step synthesis of ordered mesoporous organosilicas;[13c,k] in the case of thiol-functionalized materials, this would lead to improved metal-binding properties, at least if thiol oxidation into disulfide might be avoided by using for instance deoxygenated neutral or acid media.

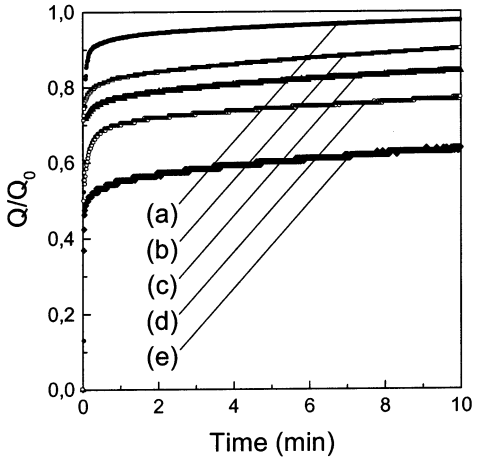

Figure 4. Protonation kinetics for APS−SBA-15 (10 mg) in 25 mL HCl solutions. The initial concentration of protons was adjusted to obtain various $H^+/R-NH_2$ ratios: (a) 44%; (b) 58%; (c) 66%; (d) 73%; (e) 100%. Q and Q_0 values are defined as in Figure 3.

3.3. Factors Affecting Diffusion inside the Organically Modified Materials. The rate of protonation of mesoporous APS materials was studied according to the same procedure as that applied to investigate kinetics of acid−base reactions in amorphous silica gels grafted with aminopropyl groups, that is, by adding a suitable amount of protons in a APS suspension and monitoring in situ their consumption as a function of time by fast pH measurements.[18] Typical kinetic curves are depicted in Figures 3 and 4, respectively, for APS−MCM-48 and APS−SBA-15 materials, with use of HCl as the acid reactant. They have been obtained at various initial acid to $\equiv Si-C_3H_6NH_2$ concentration ratios and Q_0 is the theoretical maximal amount of protonable amine groups (i.e., the starting amount of protons in the medium) while Q represents the amount of protonated $\equiv Si-C_3H_6NH_3^+,Cl^-$ functions at time t. They clearly show very fast reaction rates up to about 40−50% of theoretical completion (total amount of amine groups in the material), these filling levels being reached within the first few seconds of experiment. This sharp evolution was followed by a dramatic decrease in the protonation speed after 2 min of equilibration, which is noticeable in Figures 3 and 4 by nearly flat variations of Q/Q_0 ratios in the 2−10-min lapse of time. These sluggish reaction rates were even lower than those reported for protonation of amine-functionalized amorphous silica gels in the time scale corresponding to the 50−100% completion range.[18] Such a significant difference is rather surprising since materials with uniform pore structure, such as ordered mesoporous organic−

inorganic hybrids, usually exhibit superior binding properties and reactivity.[3,4,12−17] In the present case, one should consider the overall pathway of the protonation reaction that involves charge formation (propylammonium, counterbalanced by Cl^- anion) on the walls of cylindrical mesopores. These electronic charges are well-arranged in space and as concentrated as protonation is going on; it might induce some local electric field acting as a shield liable to hinder further penetration of charged species (i.e., H^+, Cl^-) in the mesoporous structure at a given occupancy level. The explanation is sustained by the fact that large-pore materials were affected to a lesser extent by this limitation (e.g., compare the slope of curve "g" in Figure 3 with that of curve "e" in Figure 4, in the 2−10-min lapse of time), as charges separated at a longer distance give rise to weaker electric fields. It has been checked that materials remain porous after extensive protonation (specific surface areas measured above 300 $m^2\ g^{-1}$), to exclude a major contribution of steric hindrance. The hypothetical "charge effect" would be even less in amorphous materials because of charge distribution in a more randomly way than in ordered solids, agreeing with the 100% completion of protonation that was previously reported in these materials.[18]

Influence of structure type on protonation kinetics was investigated with using the five mesoporous APS materials and one amorphous APS sample (displaying an average pore size of 60 Å), by measuring the speed of proton consumption with time from an initial acid to $\equiv RNH_2$ concentration ratio close to 50%. In water, reactions were extremely fast for all mesoporous solids (>80% protonation in less than 2 s), with dramatic improvement with respect to corresponding amorphous solids, except for APS−MCM-41(A) which behaved in a way similar to the amorphous amine-grafted material (Figure 5A). So a slow rate is explained by the blocked-pore structure of APS−MCM-41(A), arising from hierarchical polymerization of APTES inside the mesopores, which led to loosing the advantage of the uniform pore structure and performed similar to amorphous materials. The same experiments have also been performed in ethanol (Figure 5B) because the chemical stability of APS is known to be higher in this medium than in water (restricted hydrolysis damage).[18] In this case, the protonation kinetic curves passed through the origin whereas they started at Q/Q_0 values of about 0.20−0.25 in an aqueous medium due to partial leaching of aminopropylsilicate groups in solution, as already observed with amorphous APS.[18] The curves were also better defined, probably because of the higher stability of the material than in water, in which structure damage can occur upon hydration.[32b] Once again all mesoporous APS materials gave rise to protonation faster than amorphous APS, except the APS−MCM-41-(A) sample for the same aforementioned reason. Distinction between them leads to the general trend of faster kinetics with materials displaying larger pore apertures and smaller particle size. In addition, protonation of mesoporous APS in ethanol was considerably slower than that in water (comparison of inset of Figure 5B with Figure 5A). This can be explained by the bigger particle sizes observed when APS materials are dispersed in the organic solvent, whereas the packed aggregates are much more broken into smaller particles when they are dispersed in an aqueous medium. Different sizes of solvated reactants might also explain this different behavior when changing from water to ethanol. Other solvent effects on the rate of reactions involving amine-functionalized mesoporous materials have been reported, especially in catalytic applications.[20b]

Size of counteranion (X^-) is expected to affect protonation of aminopropyl groups by an acid HX in a confined medium because this anion must fit inside the structure to neutralize the positive charge arising from ammonium formation (eq 2).

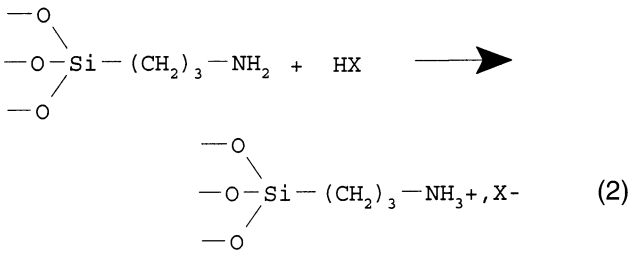

(2)

The use of acids with a large associated anion can induce low protonation yields due to steric constraints and can also result in slower kinetics as diffusion of both H^+ and X^- to the active sites located in the porous material is the rate-determining step of the protonation process. Figure 6 compares the protonation rates of APS−MCM-41(A) by HCl, trifluoroacetic acid, and picric acid. It shows noticeably slower reaction when using an acid with a larger associated anion because of slower diffusion in the microporous environment. Similar trends were observed with other small-mesopore APS samples, but differences were less marked than with APS−MCM-41(A) because of the absence of blocked pores, allowing easier diffusion. No distinguishable effect of anion size has been evidenced during protonation of large-mesopore APS materials in the time scale of the experiment due to too fast reaction rates (>80% completion in <2 s).

Structure and porosity of materials also dramatically affect the speed of metal ion trapping by ordered mesoporous organosilicas. These effects have been investigated on both APS and MPS solids. Complexation kinetics have been characterized for Hg^{II} in MPS in an aqueous medium and for Cu^{II} in APS in ethanol. Because of relatively fast uptake rates, the consumption of metal ions in solution was monitored in situ in a stirred medium by an electrochemical method based on the rotating disk electrode. Dispersion of hydrophobic MPS solids in aqueous solutions required ultrasonic treatment for several minutes prior to Hg^{II} addition, to ensure appropriate wetting of porous particles.

Figure 7A depicts the results of the kinetics experiments that have been performed to characterize mercury uptake by MPS mesoporous materials. The uptake rates are significantly lower than those for protonation of APS, and the influence of the material type is much more discriminatory. One can distinguish clearly three different behaviors: (1) fastest diffusion was observed in the large-pore mesoporous solids that were characterized by 100% accessibility to the binding sites (MPS−SBA-15 and MPS−MCM-41(C)); (2) ordered materials with smaller pore size but containing the mercaptopro-

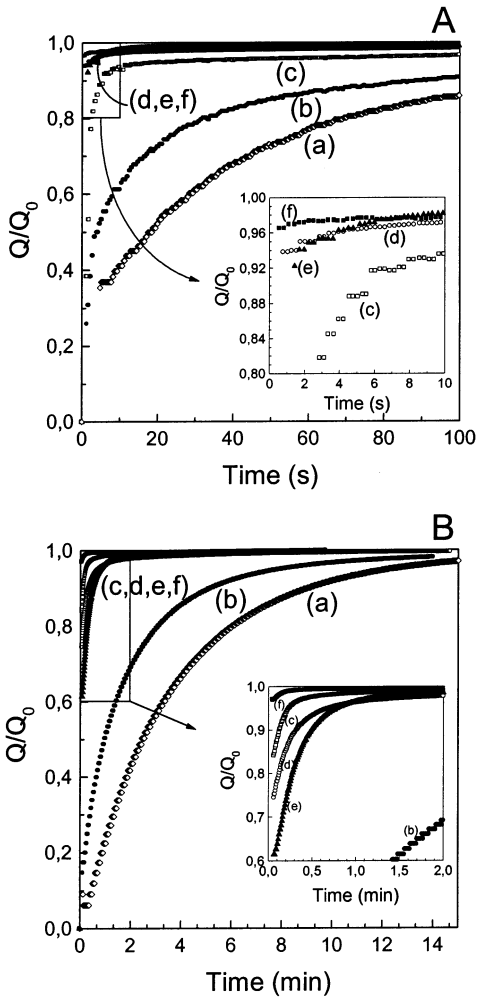

Figure 5. Effect of the structure of materials on the protonation kinetics of APS. (A) Protonation kinetics for (a) APS-G60 (13.3 mg), (b) APS−MCM-41(A) (10 mg), (c) APS−MCM-41(B) (11.2 mg), (d) APS−MCM-48 (10 mg), (e) APS−MCM-41(C) (12 mg), and (f) APS−SBA-15 (15 mg), in 25 mL aqueous solutions in which 120 μL of 0.104 M HCl has been added at $t = 0$. The amount of each material has been adjusted to ensure a initial ratios "proton-to-accessible amine groups" equal 0.5. (B) Same as (A) but the experiments have been carried out in ethanol (96%) instead of water. Insets: enlargements at early times of the experiments.

pyl ligands essentially located on the mesopore walls (MPS−MCM-41(B) and MPS−MCM-48) displayed lower reaction rates because of somewhat restricted mass transfer with respect to large-pore structures; (3) lowest uptake efficiencies were observed with the amorphous organosilica gel and the MPS−MCM-41(A) sample containing the thiol functions located within the whole mesopore volume and not only on its walls (hierarchical polymerization), as explained by stronger steric constraints and probably also by higher hydrophobicity due to the high organic group contents. This latter hypothesis is sustained by the rather slow adsorption of water on mercaptopropyl-functionalized silicas.[13o] Similar trends were observed upon evaluation of the binding properties of MPS materials in 0.5 M HCl (where Hg^{II} is mainly in the form of $HgCl_4^{2-}$ and $HgCl_3^-$), except that Q_0 values were slightly lower because of competitive action of Cl^- species against the S−Hg bond. No significant differences in the reaction rates were observed when the Hg^{II} speciation in solution was changed, in agreement

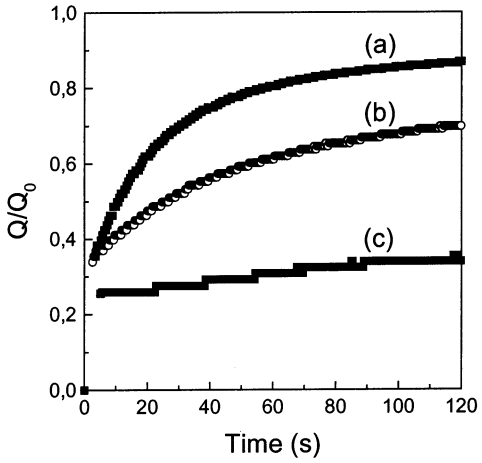

Figure 6. Effect of the counteranion size on the protonation kinetics of APS materials: evolution of proton consumption during reaction of 10 mg of APS−MCM-41(A) in a 25 mL aqueous solution containing initially 4×10^{-4} M of hydrochloric acid (a), trifluoroacetic acid (b), or picric acid (c).

with the similar adsorption rates for $Hg(OH)_2$ and HgI_4^{2-} that have been reported previously for self-assembled mercaptan on mesoporous silica.[13g] Figure 7B indicates that such a classification between large- and small-pore ordered mesoporous solids and corresponding amorphous materials is also valid for Cu^{II} binding on APS materials. This reaction has been studied in ethanol because complexation between Cu^{II} and amine groups is more quantitative in this medium[18] and because of enhanced stability of APS as compared to that of aqueous media.

Pushing further the interpretation of kinetic data requires however one to consider particle size distribution of the adsorbent to provide more accurate comparison of diffusion processes in the porous organic−inorganic hybrids.

3.4. Kinetic Data Treatment. Attempts were made to evaluate the apparent diffusion coefficients, D_{app}, by applying in a first approximation a mathematical model based on diffusion in a sphere (eq 1).[28] This model was utilized previously to characterize mass-transfer reactions in amorphous APS and MPS materials.[18] It was chosen here to obtain D_{app} values characteristic of diffusion processes in ordered organosilicas, which can be easily compared to those measured with corresponding amorphous solids. This model is not perfectly suited to the mesoporous systems as diffusion in cylindrical channels is expected to be linear. However, the mesoporous materials used here are in the form of aggregates (ill-shaped but considered roughly as spherical), displaying average particle size greater by 1−2 order(s) of magnitude than the individual crystallites. These individual crystallites are randomly arranged in space, so diffusion processes in the aggregates are mainly governed by three-dimensional mass-transfer paths. Calculation of D_{app} values was thus made on the basis of this acceptable approximation, by fitting the kinetic curves using eq 1 and measuring the particle size distribution. To obtain reliable data, the average particle size was measured in the same conditions as those applied in the kinetic experiments. It should be reminded that two other approaches were previously applied to fit experimental data of mercury ion adsorp-

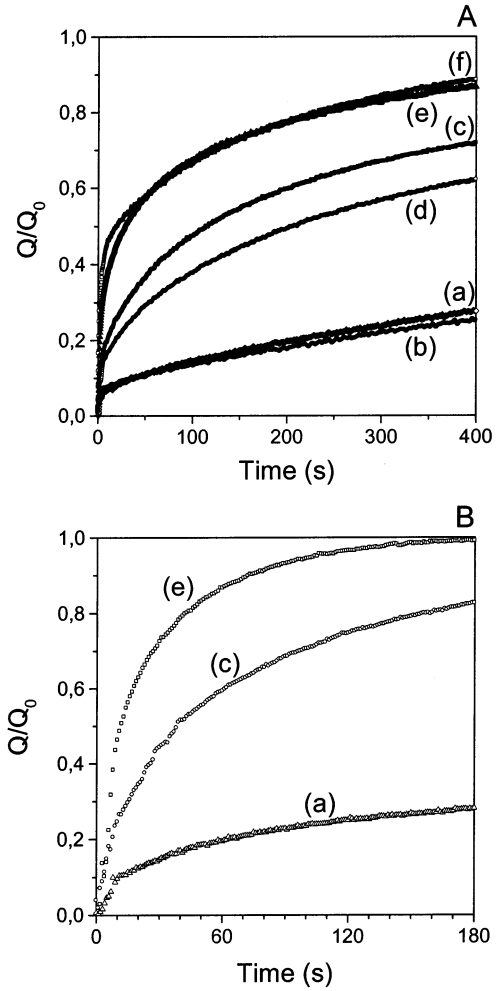

Figure 7. (A) Uptake of Hg(II), as a function of time, by (a) MPS-G60, (b) MPS−MCM-41(A), (c) MPS−MCM-41(B), (d) MPS−MCM-48, (e) MPS−MCM-41(C), and (f) MPS−SBA-15, from a 1.9×10^{-4} M $Hg(NO_3)_2$ solution (in 0.1 M HNO_3); Hg(II) was in slight excess with respect to the −SH groups; Q_0 is the maximum amount of accessible −SH groups (as given in Table 3). (B) Uptake of Cu(II), as a function of time, by (a) APS-G60, (c) APS−MCM-41(B), and (e) APS−MCM-41(C), from an ethanol (96°) solution containing initially 1.0×10^{-3} M $Cu(NO_3)_2$; Cu(II) was in excess with respect to the $-NH_2$ groups; Q_0 is the maximum amount of accessible $-NH_2$ groups (as measured after 24 h of reaction).

tion on thiol-functionalized mesoporous silicas: (1) Mattigod et al.[13g] used an empirical equation characterizing chemisorption kinetics[38] and calculated corresponding kinetic constants; (2) Bibby and Mercier[13p] characterized ion diffusion kinetics in mesoprous organosilica spheres according to the shrinking core model, usually used to study diffusion in zeolites,[39] and reported diffusion coefficients in the range 10^{-11} to 10^{-10} $cm^2\ s^{-1}$.

Figure 8 compares the variation of D_{app} values associated with the protonation of amine-functionalized MCM-41 materials (the small-pore APS−MCM-41(B) and the large-pore APS−MCM-41(C)) with that corresponding to the same reaction in amorphous silica gel grafted with the same aminopropyl ligand, as a function of the extent of protonation. A spectacular difference between ordered and amorphous materials was observed. Protonation of ordered mesoporous organosilicas was extremely fast in the early times of the experiment (much faster than amorphous APS), so accurate calculation of D_{app} values was prevented at low Q/Q_0 but the apparent diffusivity of reactants (H^+,Cl^-) dropped dramatically upon progressively transforming $\equiv Si-C_3H_6-NH_2$ groups into $\equiv Si-C_3H_6NH_3^+$,Cl^- functions, to reach values by far much lower than those recorded for protonation of amorphous APS at the same occupancy levels. This effect was more critical with the small-pore APS−MCM-41(B) solid, as illustrated by D_{app} values decreasing more rapidly when increasing Q/Q_0, as compared to the large-pore APS−MCM-41(C) sample for which the D_{app} decrease began at higher Q/Q_0 values (Figure 8). The advantage of the regular pore structure in ordered materials, in terms of high mass-transfer rates, is therefore maintained for protonation of APS samples only at low-occupancy levels (typically <40% with small-pore systems and <50% for large-pore solids, as compared to large-pore amorphous APS). Reaching the remaining unprotonated amine groups in the mesopore channels is a continuously slower process, which is extremely marked in ordered APS solids in comparison to the corresponding grafted silica gels. These results are consistent with the hypothesis of "charge effect" proposed above to explain the uncompleted protonation levels observed in these organized hybrids. Even if some active sites in the channels remained physically accessible (as demonstrated by rather high surface area, pore volume, and pore size upon reaction with a proton excess), the accumulation of charged species in the regular cylinders significantly restricts the entrance of reactants in the mesopores and hinders their diffusion to the remaining unreacted groups. Apparently, no "step-by-step" displacement of reactant was observed, for example, by proton hopping from one active site to another, because some amine groups remained inaccessible to protonation. Higher diffusion resistance by steric hindrance upon formation of $\equiv Si-C_3H_6NH_3^+$,Cl^- groups might also explain the slower diffusion rates, especially in small-pore materials.

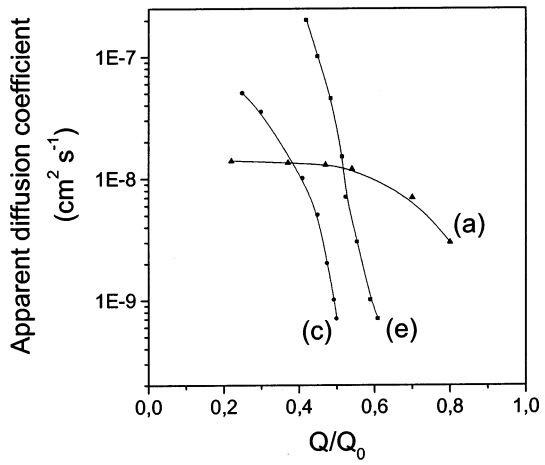

Figure 8. Variation of the apparent diffusion coefficient during protonation of (a) APS-G60, (c) APS−MCM-41(B), and (e) APS−MCM-41(C), as a function of the extent of reaction.

(38) Ungarish, M.; Aharoni, C. *J. Chem. Soc., Faraday Trans. 1* **1981**, *77*, 975.

(39) (a) Ruthven, D. M. *NATO ASI Ser., Ser. C* **1997**, *491*, 241. (b) Ruthven, D. M.; Post, M. F. M. *Stud. Surf. Sci. Catal.* **2000**, *137*, 525.

(40) Gregg, S. J.; Sing, K. S. W. *Adsorption, Surface Area and Porosity*; Academic Press: London, 1982; pp 113−120.

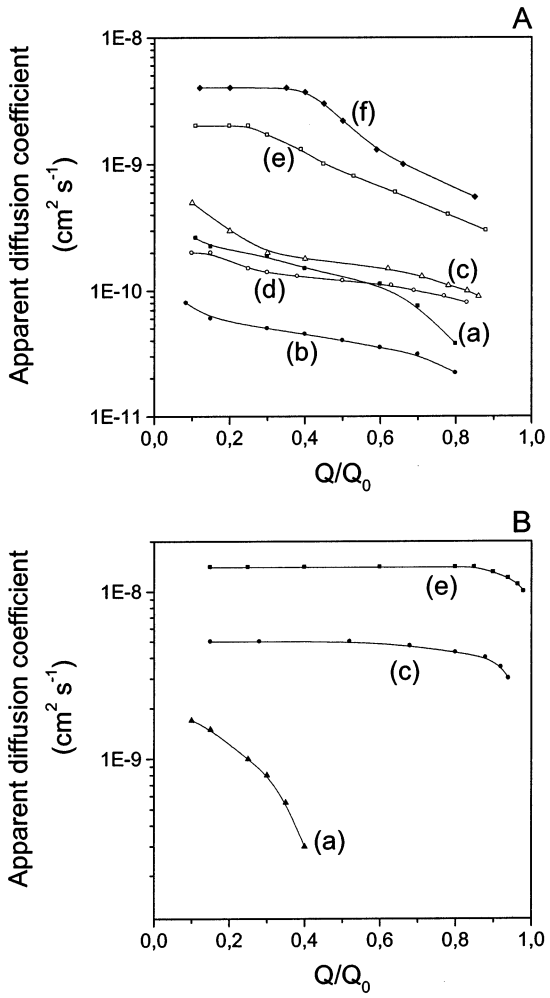

Figure 9. (A) Variation of the apparent diffusion coefficient during uptake of Hg(II) by (a) MPS-G60, (b) MPS−MCM-41-(A), (c) MPS−MCM-41(B), (d) MPS−MCM-48, (e) MPS−MCM-41(C), and (f) MPS−SBA-15, as a function of the extent of reaction. (B) Variation of the apparent diffusion coefficient during uptake of Cu(II) by (a) MPS-G60, (c) MPS−MCM-41-(B), and (e) MPS−MCM-41(C), as a function of the extent of reaction. Other experimental conditions as in Figure 7.

The apparent diffusion coefficients relative to the metal ion-binding properties of ordered APS and MPS materials were also evaluated by applying the same diffusion model to Hg^{II} uptake by MPS samples in an aqueous medium and Cu^{II} adsorption within APS solids in ethanol. D_{app} values have been calculated at various occupancy levels and plotted as a function of Q/Q_0, as illustrated in Figure 9. Contrary to those from protonation of APS, D_{app} values associated with metal binding were less subject to large variation with the occupancy level. They were still decreasing upon rising Q/Q_0, but this tendency was very much less marked than that for protonation of APS. Such a slow decrease in diffusivity is explained by steric constraints that are more important as fast as metal adsorption proceeds, as sustained by the decrease in total pore volume of the materials upon filling with the heavy metal (Table 3). D_{app} values for metal ion binding in ordered materials were sligthly lower than those corresponding to protonation (at least at completion <50%). Those values recorded for large-pore SBA-15 and MCM-41(C) were found to be higher than those corresponding to amorphous solids of similar pore size, by about 1 order of magnitude. On the other hand, the ordered solids displaying a 2-fold narrower pore size (MCM-41(B) and MCM-48) gave rise to D_{app} values of the same order of magnitude as the amorphous sample, confirming again the major importance of the uniform structure to ensure fast diffusion rates. No significant difference was observed between the MCM-41 and MCM-48 structures (Figure 9A). Finally, MPS-MCM-41(A) containing mercaptopropyl groups in most of the mesopore volume led to substantially inferior kinetics, so improvement due to the ordered mesopore structure is valid only if the channels remain open to the external solution upon grafting. Note that the rather low D_{app} values obtained for Hg^{II} binding in MPS−MCM-41(A) and MPS−MCM-48 materials could also be partially explained by a higher hydrophobic character due to higher mercaptopropyl groups content with respect to other MPS samples (Table 2). Diffusion kinetics associated with the uptake of Cu^{II} by APS materials were following similar trends.

In agreement with the rather long times to obtain complete filling of the organosilicas, and with the decrease in pore volume concomitant to the uptake process, the apparent diffusion coefficients were found to decrease as far as reaction was going on, the variation being a function of the material type, the ligand density, the analyte properties, and the nature of reaction involved. This experimentally observed trend is apparently not compatible with some recently reported results on mercury ion adsorption by thiol-functionalized mesoporous silica microspheres for which synergistic acceleration of the uptake rate was found with increasing metal ion loading.[13p] This rather surprising evolution had been explained by the authors by limited ion permeation at the beginning of the experiment because of the hydrophobic environment of mesopores loaded with the thiol groups. It should be reminded that, for the Hg^{II} adsorption experiments performed here with MPS materials, the solid particles were dispersed in water under ultrasonic treatment for several minutes prior to contacting the reactant solution. Under these circumstances, hydration of the mesopores could have been better realized so that the overall sorption process is thought to be less affected by slow infiltration of the aqueous phase in the pore channels and would be directly related to the intrinsic diffusion of reactants inside the porous structure. This possible explanation is supported by the fact that the D_{app} values evaluated here for grafted mesoporous silicas are much higher than those reported previously (more than 1 order of magnitude) for the same kind of organosilicas obtained by the co-condensation route.[13p] Moreover, protonation of—and copper binding in—the more hydrophilic APS materials gave rise to observation of the same trends of decreasing diffusion rates when reaction proceeds, confirming the difficulty for the reactant to reach the remaining unreacted active centers at high-occupancy levels.

4. Conclusions

Grafting five mesoporous silicas with either aminopropyl or mercaptopropyl groups leads to ordered organic−inorganic hybrid materials whose reactivity is strongly affected by their structure, porosity, density of organic groups, reaction type, and analyte size. In

general, accessibility to the active sites is better and mass-transfer kinetics are faster than those in the corresponding amorphous grafted materials, but this conclusion must be restricted in some cases.

Protonation of aminopropyl groups grafted on porous silica samples is faster in the first half of reaction when using ordered mesoporous solids instead of amorphous materials, but it becomes slower at higher reaction degrees, resulting even in less-than-complete accessibility to the acive sites at equilibrium. These limitations are due to the concentration of charged moieties in a well-structured environment, which limits the progression of reactants inside the regular mesopores. Binding heavy metal species in ordered organosilicas (e.g., Hg^{II} in MPS or Cu^{II} in APS) was also improved in comparison to that of amorphous silica gels grafted with the same ligands. Accessibility to the binding sites and diffusion rates inside the mesostructure were however affected by pore size of the starting material as well as ligand density in the mesopores: (1) 100% accessibility was always observed for large-pore ordered materials (~60 Å), while decreasing pore size and increasing ligand population resulted in incomplete filling status because some organic groups remained unavailable to the solution-phase reactants due to steric constraints; (2) the uniform mesoporous structure of the ordered solids imparts to the organic−inorganic hybrids faster kinetics associated with the uptake of metal ion species from diluted solutions, and this effect is markedly more advantageous when using large-pore materials; (3) the advantage of molecular sieve silicas over the amorphous ones disappears when the grafting process is performed in the presence of trace water (leading to some hierarchical polymerization of the grafting agent in the mesopores), which can lead in this case to superior binding properties for the amorphous materials.

Better accessibility and lower diffusion resistance in ordered mesoporous organic−inorganic hybrid materials, in comparison to their amorphous counterparts, make them interesting for possible improvements in many applications (faster remediation processes, lower response time of sensors, greater electrochemical sensitivities, higher catalytic efficiency and turnover, etc.).

Acknowledgment. We are grateful to M. Mahé and Dr. J. Parmentier for the synthesis of MCM-41(C) and MCM-48 samples, respectively. We also appreciate the help of J. Cortot for ICP-AES measurements and J.-P. Emeraux for recording XRD spectra. Prof. M. J. Hudson is gratefully acknowledged for providing us with the MCM-41(B) sample.

Supporting Information Available: XRD patterns and nitrogen adsorption−desorption isotherms for samples MCM-41(A), MCM-41(B), MCM-41(C), SBA-15, and MCM-48 (PDF). This material is available free of charge via the Internet at http://pubs.acs.org..

CM021310E